

## Ion Hole Equilibrium and Dynamics in One Dimension

I H Hutchinson

*Plasma Science and Fusion Center,  
Massachusetts Institute of Technology,  
Cambridge, Massachusetts, 02139, USA*

Electrostatic solitary waves with negative potential (ion holes) are analyzed theoretically using a generalization of the treatment recently developed for slow electron holes. It is shown that an often-cited criterion for their existence is mistaken and they can in fact exist for a wide range of ion to electron temperature ratios. Shifts of the hole velocity  $v_h$  relative to the ion distributions systematically decrease the permitted hole depths, which become extremely small by  $v_h/v_{ti} \sim 2$ . Ion holes are usually unstably accelerated by electron reflection forces which are calculated numerically and analytically for the resulting asymmetric potential structure. The timescale of this acceleration is proportional to the ion plasma period, and generally longer than the ion bounce time in the potential well. Thus, ion holes behave like approximately rigid entities and even when unstable can survive much longer than the typical transit time of a satellite, so as to be observable.

## I. INTRODUCTION

A solitary negative electrostatic potential structure sustained in a plasma by a deficit of trapped ions is called an ion hole. Ion hole theory springs from Bernstein, Greene, and Kruskal (BGK mode) equilibrium analysis<sup>1</sup>, and from its subsequent development<sup>2-4</sup>, which accompanied ion hole observations in laboratory experiment<sup>5,6</sup> and in numerical simulation<sup>7-10</sup>. More recently, unambiguous identification of the polarity of solitary structures in space observations has shown that ion holes occur widely at the Earth's bow shock<sup>11</sup>, the Plasma Sheet<sup>12</sup>, and in the near-Sun solar wind<sup>13</sup> as well as in the auroral region<sup>14</sup>. These observations, together with recent related developments in the theory and observation of positive potential solitary waves (i.e. *electron holes*)<sup>15,16</sup>, provides motivation to revisit ion hole theory.

The mechanisms that are expected to produce ion holes are kinetic ion streaming instabilities (e.g.<sup>17</sup>) including ion-ion, Buneman, and ion-acoustic instabilities; but the present work reports on ion holes' equilibria once formed and subsequent dynamics, rather than on formation mechanisms. The theory depends upon an assumption that ion holes persist long enough to be treated as quasi-static Vlasov equilibria, in which case the velocity distribution function is constant on particle orbits. But whether that assumption is justified itself depends on the fate of an ion hole regarded as a composite object accelerating under the influence of the rest of the plasma. Although trains of ion holes are often observed, the present analysis concentrates on solitary holes in a prescribed background plasma. The treatment draws heavily on related theory of electron hole dynamics<sup>18,19</sup>, but the large mass difference makes interaction with the opposite charge species more important for ion holes.

Section II explains the generalized notation in terms of attracted and repelled species and how reflection affects the repelled distribution function. Section III addresses hole equilibria in the presence of symmetric repelled species distributions and calculates the criteria for their existence, correcting an important prior error in the literature. Section IV shows how to calculate the momentum balance of a hole when it is subject to acceleration arising from asymmetric reflection, and gives analytic values for the acceleration growth rate from initial equilibrium. Discussion of the significance and limitations of the present analysis is given in Section V.

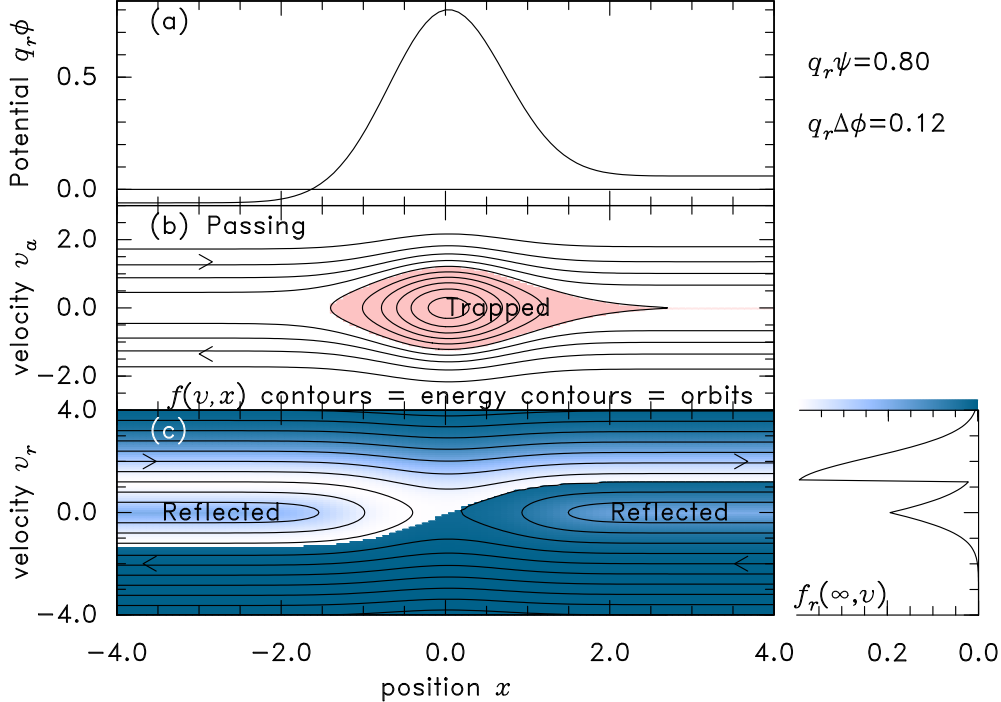


FIG. 1. Generic phase-space hole structure. (a) potential, (b) attracted species phase space density contours, (c) repelled species contours.

## II. GENERAL PHASE-SPACE HOLE EQUILIBRIA

Electron holes can, and often do, have speeds much higher than ion thermal speed, allowing them to be considered unaffected by ion interactions. When this is not the case they are considered “slow”. By contrast, ion holes exist only when the spread of the ion distribution function  $f_i(v)$  in the hole rest frame makes  $f_i(0) \neq 0$ . The ion velocity spread is much smaller for physical mass ratios than the electron velocity spread; so ions are thus practically always slower than electrons and ion holes are always “slow” in the sense that they reflect some of the repelled species: electrons. To treat such “slow” situations, and transfer intuition and calculation from electron holes to ion holes it is convenient to treat both ions and electrons on an equal footing as follows.

We consider a local region of potential  $\phi(z)$  having only a single stationary point ( $\frac{\partial\phi}{\partial z} = 0$ ) at  $z = 0$ , and zero slope at  $|z| \rightarrow \infty$ . The local region is called the hole, as illustrated in Fig. 1(a). The hole is (initially) at rest  $\frac{\partial\phi}{\partial t} = 0$  in its frame of reference. Taking the zero of potential to be  $(\phi(+\infty) + \phi(-\infty))/2 = 0$ , the sign of  $\phi(0)$  (which is necessarily minus the sign of  $d^2\phi/dz^2|_0$ ) attracts particles toward  $z = 0$  if their charge is opposite that of  $\phi(0)$ , or repels

them if it is the same. We will use subscripts  $a$  and  $r$  to denote attracted and repelled. So, for an ion hole ( $\phi(0) \leq 0$ ),  $i \leftrightarrow a$ , and  $e \leftrightarrow r$ . We use units that are non-dimensionalized using the mass of the species under consideration but the (effective external) temperature  $T_a$  of the attracted species. Thus, time is measured in units of  $\omega_p^{-1} = \sqrt{\epsilon_0 m / n q^2}$ , velocity in units of  $\sqrt{T_a / m} = 1$ , length in units of  $\lambda_{Da} = \sqrt{n_\infty q^2 / \epsilon_0 T_a}$ , potential in units of  $|q| T_a$ . Quantities without  $a$  or  $r$  subscripts here correspond to whichever species is under consideration. For example, electron and ion velocities are normalized respectively to their (different) thermal velocities  $\sqrt{T_a / m_{e/i}}$ . For simplicity we regard the charge magnitudes  $|q|$  to be the same for both species (singly charged ions), so outside the hole, neutrality gives  $n_{a\infty} q_a^2 = n_{r\infty} q_r^2$ . The normalized density of both in the absence of a hole is  $n_\infty = 1$ , and the normalized magnitude of charge is  $|q| = 1$ . The units of time (and velocity) are different for different species by the square root of the mass ratio. It is convenient to introduce an abbreviation for the normalized potential energy of the repelled species:  $\varphi \equiv q_r \phi$  which is always positive at  $z = 0$ . We denote the maximum repelled potential energy as  $\psi$ , always positive. We allow for the possibility that there is a potential difference  $\Delta\varphi = \varphi(+\infty) - \varphi(-\infty)$  across the hole, but not that the difference is so great that it eliminates the local maximum of  $\varphi$ .

Provided the transit time of the particles is short compared with any hole potential changes (so  $\phi$  is effectively time-independent in the hole frame), the repelled species' velocity distribution is determined by the constancy of  $f_r$  on orbits (Vlasov equation), the conservation of energy ( $\mathcal{E}_r = v^2/2 + q_r \phi = v^2/2 + \varphi$ ), and the value of  $f_r(v) = f_r(\sqrt{2[\mathcal{E}_r - \varphi]})$  at  $|z| = \infty$ . The velocity distribution of only the *untrapped* particles of the attracted species is determined by distant conditions; those particles have  $\mathcal{E}_a = v^2/2 - \varphi \geq -|\Delta\varphi/2|$ . The attracted species particles with  $\mathcal{E}_a < -|\Delta\varphi/2|$  are trapped; their orbits are localized in the hole; and the distribution on them is determined by the initial conditions of formation of the hole. Fig. 1 (b) and (c), illustrate the attracted and repelled species' phase-space distribution contours for a case where the incoming distributions are Maxwellians of the same temperature but the repelled velocity distribution is shifted (in the hole frame) by a normalized velocity of  $\bar{v}_r = 1.2$ . This shift causes discontinuities in  $f_r$  at the boundary between passing and reflected orbits. The resulting ( $z \rightarrow \infty$ ) distribution is illustrated in the side panel, which indicates the intensity calibration for the repelled species contours.

It is conceptually and numerically advantageous to regard the attracted species as consisting of a reference distribution given by the passing particles but including a flat distribution

(independent of  $v$ ) of trapped particles, matching the untrapped distribution at their join where total energy in the hole frame,  $\mathcal{E}$ , is  $-|\Delta\varphi/2|$ . The trapped region is pink in Fig. 1(b). This “flat-trapped” distribution  $f_f(v)$  governs the attracted species when there is no “hole” in the distribution. It is what would arise if the hole potential were (hypothetically) grown infinitesimally slowly. By itself, it is generally unable to sustain the potential self-consistently through Poisson’s equation, and requires an additional contribution on trapped orbits only,  $\tilde{f}$ , which is negative, and represents the deficit of the phase-space density.  $\tilde{f}$  is responsible for the required charge density with sign the same as  $\phi$  near the hole center. The corresponding particle densities  $n = \int f dv$ , are functions of  $\phi$ : repelled  $n_r$ , and attracted  $n_f + \tilde{n}$ .

Poisson’s equation for the hole is then

$$\frac{1}{q_a} \frac{d^2\phi}{dz^2} = -\frac{d^2\varphi}{dz^2} = n_r - n_f - \tilde{n}. \quad (1)$$

If we regard  $\varphi(z)$ , and  $f_a, f_r$  at  $|z| = \infty$ , as prescribed, then all terms except  $\tilde{n}$  are prescribed, and  $\tilde{n}$  is determined. Then  $\tilde{n} = \int \tilde{f} dv$  is an integral equation determining the trapped distribution deficit  $\tilde{f}$ . It is Abel’s integral equation whose known solution (on the higher  $\varphi(\pm\infty)$  side) is

$$\tilde{f}(v_0) = \frac{1}{\sqrt{2\pi}} \int_{|\Delta\varphi/2|}^{\psi-v_0^2/2} \frac{d\tilde{n}}{d\varphi} \frac{d\varphi}{\sqrt{\psi - v_0^2/2 - \varphi}} = \frac{1}{\sqrt{2\pi}} \int_{|\Delta\varphi/2|}^{-\mathcal{E}} \frac{d\tilde{n}}{d\varphi} \frac{d\varphi}{\sqrt{-\mathcal{E} - \varphi}}, \quad (2)$$

where  $v_0$  denotes the attracted species velocity at the center of the hole  $z = 0$  ( $\varphi = \psi$ ), which is  $v_0 = \sqrt{2(\mathcal{E} + \psi)}$ .

### III. EQUILIBRIA WITH MAXWELLIAN BACKGROUND

Suppose the repelled species velocity distribution  $f_r(v)$  is an unshifted Maxwellian in the frame of the hole. The repelled species density is then  $n_r = e^{-\varphi/\theta}$ , where  $\theta = T_r/T_a$ . Take the untrapped attracted velocity distribution to be a Maxwellian distribution with a velocity shift  $\bar{v}_a$  in the hole frame. Then the flat trapped distribution at potential  $\varphi$  is

$$f_f(v, \varphi) = \frac{1}{\sqrt{2\pi}} e^{-(\sigma_v \sqrt{2 \max(\mathcal{E}_a, 0) - \bar{v}_a})^2 / 2} = \frac{1}{\sqrt{2\pi}} e^{-(\sigma_v \sqrt{\max(v^2 - 2\varphi, 0) - \bar{v}_a})^2 / 2} \quad (3)$$

where  $\sigma_v = v/|v|$  is the sign of  $v$ , and all velocities are expressed in the hole rest frame. The integral over all velocities gives the density  $n_f(\varphi) = \int f_f(v, \varphi) dv$ .

## A. Unshifted Maxwellian attracted species

It is easy to show<sup>16</sup> that when  $\bar{v}_a = 0$ , the resulting flat-trapped density is

$$n_f = \frac{2}{\sqrt{\pi}}\varphi^{1/2} + e^\varphi \operatorname{erfc}(\varphi^{1/2}). \quad (4)$$

Poisson's equation for the hole is then

$$-\frac{d^2\varphi}{dz^2} = n_r - n_f - \tilde{n} = e^{-\varphi/\theta} - \left[ \frac{2}{\sqrt{\pi}}\varphi^{1/2} + e^\varphi \operatorname{erfc}(\varphi^{1/2}) \right] - \tilde{n}. \quad (5)$$

Denoting the (prescribed) field divergence as  $n_\varphi \equiv \frac{d^2\varphi}{dz^2}$ . We have  $\tilde{n} = n_\varphi + n_r - n_f$  which is to be substituted into eq. (2). Since that equation is linear in the density deficit, we can treat the three density terms separately and then add them up. The repelled species derivative needed for eq. (2) is  $\frac{dn_r}{d\varphi} = -e^{-\varphi/\theta}/\theta$ , and the flat-trapped contribution is  $\frac{dn_f}{d\varphi} = e^\varphi \operatorname{erfc}(\varphi^{1/2})$ .

As an illustrative choice let us suppose that  $\Delta\varphi = 0$  and the hole potential is of the form

$$\varphi(z) = \psi \operatorname{sech}^\ell \left( \frac{z}{\ell\lambda} \right). \quad (6)$$

The parameter  $\ell$  is usually taken to be 4, but we retain slightly more generality, because we can still derive closed analytic expressions. That mathematical convenience arises from the identity  $\frac{d^2}{dx^2} \operatorname{sech}^\ell x = \ell^2 \operatorname{sech}^\ell x - \ell(\ell+1) \operatorname{sech}^{\ell+2} x$ , from which we find

$$n_\varphi = \frac{d^2\varphi}{dz^2} = \frac{1}{\lambda^2} \left[ \varphi - \frac{\ell+1}{\ell} \frac{\varphi^{(\ell+2)/\ell}}{\psi^{2/\ell}} \right]; \quad (7)$$

and so

$$\frac{dn_\varphi}{d\varphi} = \frac{1}{\lambda^2} \left[ 1 - \frac{\ell+1}{\ell} \frac{\ell+2}{\ell} \left| \frac{\varphi}{\psi} \right|^{2/\ell} \right]. \quad (8)$$

To avoid divergent slope of  $\tilde{f}$  at  $\mathcal{E} = 0$ , it is necessary that  $\left. \frac{d\tilde{n}}{d\varphi} \right|_{\varphi=0} = 0$ . That condition immediately becomes

$$\frac{1}{\lambda^2} = \left. \frac{dn_\varphi}{d\varphi} \right|_{\varphi=0} = \left[ -\frac{dn_r}{d\varphi} + \frac{dn_f}{d\varphi} \right]_{\varphi=0} = \frac{1}{\theta} + 1 \quad (9)$$

The parameter  $\lambda$  is precisely the potential decay length combining repelled and attracted species screening in attracted Debye length units, because  $\lambda_{Dr}^2 = \lambda_{Da}^2 \theta$ .

Substituting the three contributions  $\frac{dn_r}{d\varphi}$ ,  $-\frac{dn_f}{d\varphi}$ , and  $\frac{dn_\varphi}{d\varphi}$  into eq. (2) we can find three corresponding contributions to  $\tilde{f} = \tilde{f}_r + \tilde{f}_f + \tilde{f}_\varphi$ . After considerable integration effort they

can be expressed in terms of the complex Faddeeva function<sup>20</sup>  $w(z) \equiv e^{-z^2} \operatorname{erfc}(-iz)$ , and the Gamma function  $\Gamma(z)$ , as follows:

$$\tilde{f}_r = -\frac{1}{\sqrt{2\pi}} \Im[\theta^{-1/2} w(\sqrt{|\mathcal{E}|/\theta})], \quad (10)$$

$$\tilde{f}_f = \frac{1}{\sqrt{2\pi}} \Re[1 - w(i\sqrt{|\mathcal{E}|})], \quad (11)$$

$$\tilde{f}_\varphi = -\frac{\sqrt{|\mathcal{E}|}}{\sqrt{2\pi}\lambda^2} \left[ \frac{2}{\sqrt{\pi}} - \frac{\ell+1}{\ell} \frac{\ell+2}{\ell} \frac{\Gamma(1+2/\ell)}{\Gamma(3/2+2/\ell)} \left| \frac{\mathcal{E}}{\psi} \right|^{2/\ell} \right]. \quad (12)$$

Eqs. (10) and (11) are equivalent to terms found by Chen et al<sup>21,22</sup>. By virtue of the condition (9), the coefficient of  $\sqrt{|\mathcal{E}|}$  in an expansion of  $\tilde{f}$  near  $\mathcal{E} = 0$  cancels to zero between the three terms. However, the term  $\propto |\mathcal{E}|^{1/2+2/\ell}$  (from  $\tilde{f}_\varphi$ ) remains. If  $\ell > 4$ , its contribution causes  $f' = d\tilde{f}/dv$  to diverge at the phase-space separatrix, i.e. as  $|\mathcal{E}| \rightarrow 0$ , which is mildly unphysical; but it avoids non-monotonic behavior which makes some other  $\varphi$  shape choices even less plausible. The standard value  $\ell = 4$  makes the bracket  $[2/\sqrt{\pi} - (15\sqrt{\pi}/16)|\mathcal{E}/\psi|^{1/2}]$ , and  $\tilde{f}'(\mathcal{E} \rightarrow 0-)$  is finite. For  $\ell < 4$ ,  $f'(\mathcal{E} \rightarrow 0-) = 0$ . These results make no approximations, but assume that  $f(v)$  is a function only of  $\mathcal{E}$ , i.e. satisfies the Vlasov equation in a steady potential. They are illustrated in Fig. 2(a).

## B. Shifted Maxwellian Attracted Species

If the attracted Maxwellian is shifted by  $\bar{v}_a \neq 0$  in the frame of the hole, then there exists no useful closed form expression for  $n_f$  at arbitrary  $\varphi$ . Numerical curves of  $n_f$  have been given elsewhere<sup>16</sup>. They decrease for non-zero  $\varphi$  as  $\bar{v}_a$  increases. Their slope at  $\varphi = 0$  can be shown by expansion<sup>3</sup> to be  $\frac{dn_f}{d\varphi} = -\frac{1}{2} \Re[Z'(\bar{v}_a/\sqrt{2})] = \Re[1 + i\sqrt{\pi}zw(\bar{v}_a/\sqrt{2})]$ , which is what determines the attracted species distant shielding length. Therefore eq. (9) is modified to become

$$0 = \frac{1}{\lambda^2} - \frac{1}{\theta} + \frac{1}{2} Z'_r(\bar{v}_a/\sqrt{2}). \quad (13)$$

This condition at  $\varphi \rightarrow 0$  (or its equivalent<sup>23</sup>) has been referred to, in many publications<sup>24</sup> based on prescribing  $\tilde{f}(\mathcal{E}) + f_f(\mathcal{E})$  rather than  $\varphi(z)$ , as the “nonlinear dispersion relation”. It is then supposed that it relates the hole’s potential amplitude, speed (relative to the attracted species), and trapped particle temperature. That is a misleading perspective, whether for electron holes or ion holes, because it adopts a particular form for the entire

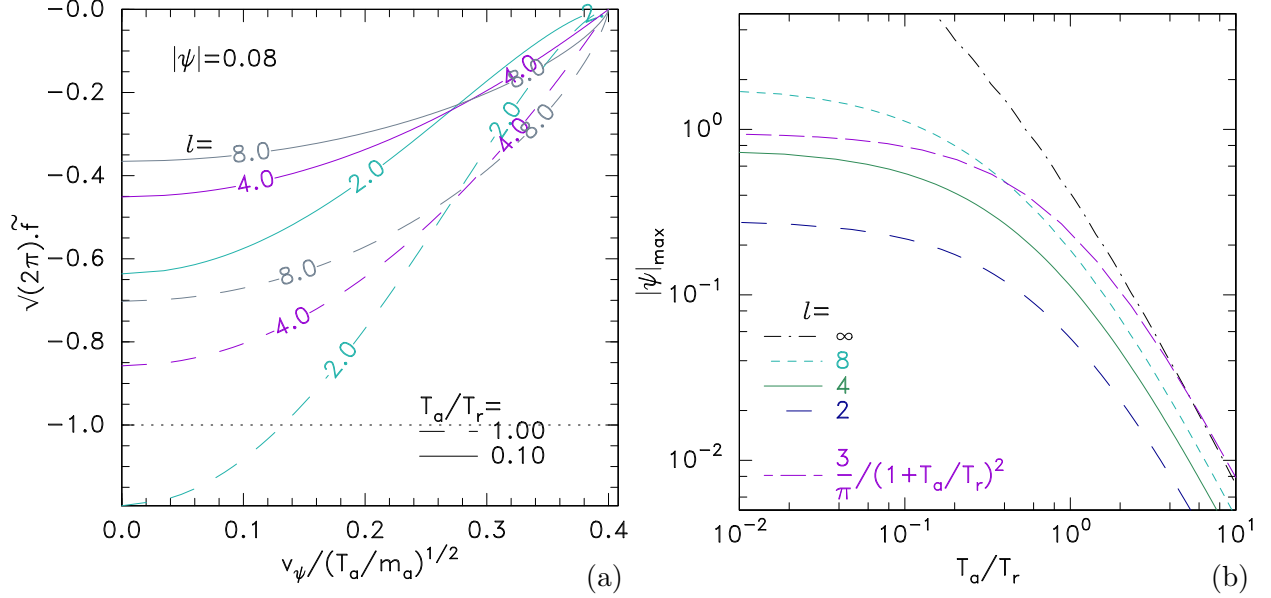


FIG. 2. Examples of ion (or electron) holes with unshifted background Maxwellian distributions of both species. (a) the required trapped deficit at  $z = 0$ ,  $\tilde{f}(v_\psi)$ , to produce a hole of the form  $\varphi = \psi \operatorname{sech}^l(z/l\lambda)$  with  $l = 2, 4$ , or  $8$ , for two ratios of the attracted to repelled species ratio ( $T_a/T_r$ ). (b) The maximum  $\psi$  value permitted by non-negativity, as a function of temperature ratio, showing a wide allowable range of  $T_a/T_r (=1/\theta)$  at low  $\psi$ . The comparison curve  $\frac{3}{\pi} / (1 + T_a/T_r)^2$  represents an analytic estimate (to first order in  $\psi$ ) for a waterbag deficit profile: the least constraining of the models described in Appendix A.

trapped distribution (negative temperature Maxwellian), which strongly constrains the potential shape. Actually the relative shape of the hole can have a whole range of widths upward from a minimum determined by non-negativity of  $f$  and the value of  $\psi$ . Avoiding divergent  $\tilde{f}$ -gradients requires primarily that  $\varphi$  decays at large distances (small  $\varphi$ ) with second derivative length scale ( $\lambda$ ) satisfying eq. (13); and the trapped deficit  $\tilde{f}$  must be consistent with the rest of the potential shape.

A hole's speed  $|\bar{v}_a|$  relative to the attracted background must not be so great that the combined particle terms at  $|z| \rightarrow \infty$  (small  $\varphi$ ),  $\frac{dn_r}{d\varphi} - \frac{dn_f}{d\varphi} (= -1/\theta + \frac{1}{2}Z'_r)$ , become positive, otherwise (13) cannot be satisfied for real  $\lambda$ . That requires  $-Z'_r(\bar{v}_a/\sqrt{2})/2 > -1/\theta$ . Speed must also be small enough that the background attracted species distribution at the hole speed is non-zero, otherwise there is no phase-space density there, in which it could be a hole. The hole amplitude  $\psi$  is limited only by the non-negativity of  $f(v)$ , which we shall



treat in a moment.

A misunderstanding related to eq. (13) is the belief<sup>25</sup>, often repeated<sup>2,3,6,8,11,26–30</sup>, that for an ion hole to exist (“a solution of the nonlinear dispersion relation [to] exist[s]”) the species’ temperature ratio must satisfy  $T_r/T_a = T_e/T_i = \theta > 1/|\min(-Z'_r(\bar{v}_a/\sqrt{2})/2)| \simeq 3.5$ . The minimum of  $-Z'_r/2$  over all real arguments is -0.285 which is where the value 3.5(=1/0.285) comes from. But in fact there is a sign error in this published criterion. At the  $-Z'_r/2$  minimum eq. (13) requires  $-0.285 > -1/\theta$  for  $\lambda$  to be real.<sup>31</sup> That is  $\theta < 3.5$ , not  $\theta > 3.5$ .

In any case, the minimum of  $-Z'_r/2$  occurs at a speed  $\bar{v}_a = 2.13$ ; so this corrected criterion is relevant only for a hole on the tail of the attracted species’ velocity distribution, and not at all to more typical holes lying deeper within the bulk population, where  $-Z'_r/2$  is positive. The important effect of finite response of the repelled species is instead that it increases the required trapped species deficit  $|\tilde{f}|$ , and makes the requirement of non-negativity more stringent. Extensive calculations of ion hole equilibria have been given by Chen, Thouless, and Tang<sup>21</sup>, who note that they are counter-examples to the erroneous criterion. Moreover recent observations by Wang *et al.*<sup>12</sup> show that ion holes in the Plasma Sheet are not subject to the erroneous criterion, since they occur where  $T_e/T_i \lesssim 0.3$ .

Detailed calculations of hole structure with  $\text{sech}^l$  potential shape and unshifted distributions, illustrating the actual hole feasibility, are given in Fig. 2. The mathematics (equations 10 to 12) is identical for ion and electron holes when expressed in our present normalized units. Non-negativity of the trapped distribution requires that  $\tilde{f} > -f_a(\mathcal{E} = 0)$ , which is  $\sqrt{2\pi}\tilde{f} > -1$  for an unshifted Maxwellian, marked with a dotted line in Fig. 2(a). Thus, of the six cases shown there, only the  $l = 2$  case with equal temperatures  $T_a/T_r = 1/\theta = 1$  is impossible. All the others are possible equilibria. If  $\psi$  were decreased, none would be impossible; if it were increased, more cases would require unphysical negative  $f_a$ .

Fig. 2(b) shows the maximum allowable hole amplitude  $\psi_{max}$  as a function of  $T_a/T_r = 1/\theta$ , for several values of  $\ell$ . That maximum occurs when the trapped distribution  $f_f + \tilde{f} = f(0) + \tilde{f} = f(0) + \tilde{f}_r + \tilde{f}_f + \tilde{f}_\varphi$  reaches zero at  $z = v = 0$  (i.e. at  $\mathcal{E} = -\psi$ ). The root of this expression is found numerically. In addition, to show that the contradiction of the widely cited criterion is not somehow attributable to the fact that the “integral equation” method is used to obtain it, Fig. 2(b) also includes the upper boundary of  $\psi$  allowed by non-negativity, obtained analytically using the “differential equation” method for a prescribed  $f_f + \tilde{f}$  shape. The  $\tilde{f}$  shape for this curve is two-level (waterbag), which of all the monotonic

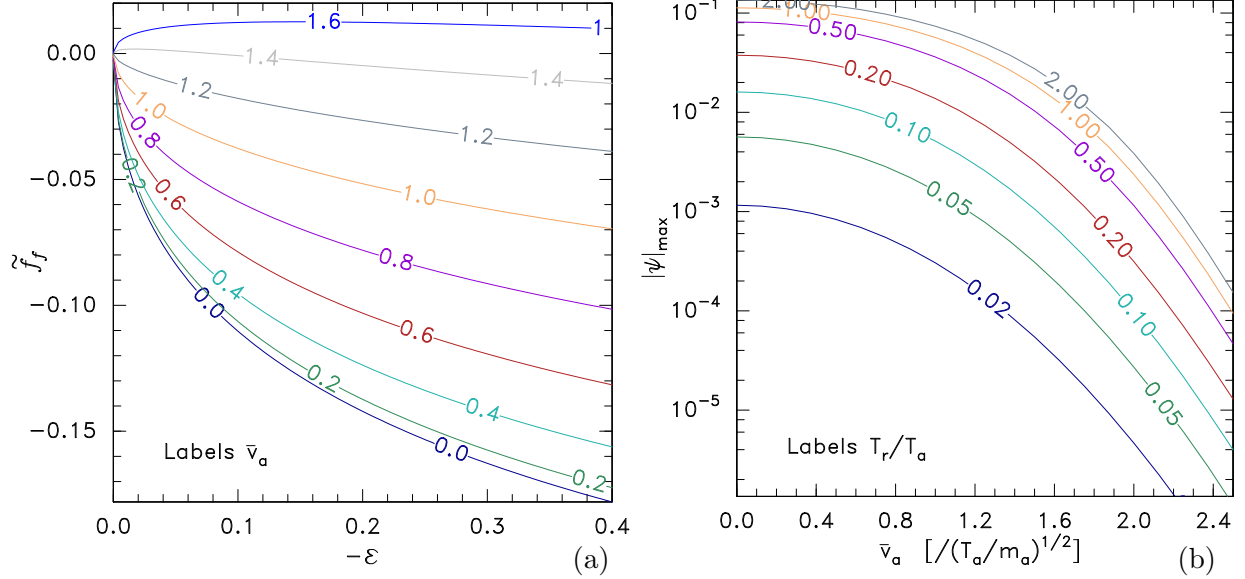


FIG. 3. (a) The contribution arising from the flat-trapped distribution to  $\tilde{f}(\mathcal{E})$ : the required trapped distribution deficit as a function of energy. Line labels indicate Maxwellian shift  $\bar{v}_a$ . (b) The hole potential amplitude permitted by non-negativity of  $f$  as a function of attracted Maxwellian velocity shift. The potential profile uses  $l = 4$ . Line labels indicate temperature ratio  $T_r/T_a = \theta$ .

“power deficit” models<sup>32</sup>, allows the highest  $\psi_{max}$ . See Appendix A for details. Since the resulting expression,  $\psi_{max} = \frac{3}{\pi}/(1 + T_a/T_r)^2$ , approximates the  $n_f - 1$  and  $n_r - 1$  as linear in  $\varphi$ , it is accurate only to first order in  $\psi$ . When  $\psi_{max}$  is small, because  $T_a/T_r \gtrsim 1$ , it agrees remarkably well with the  $\text{sech}^l$  model, especially for large  $l$ , which is the potential shape that is least constraining. The curve for a Gaussian potential shape appearing in Chen, Thouless, and Tang<sup>21</sup>[Fig 1b] is very similar to the  $l = \infty$  curve, both of which might over-estimate the maximum allowed  $\psi$  at  $T_a/T_r \lesssim 1$ , because their divergent gradient at  $\mathcal{E} = 0$  is unphysical.

A background distribution velocity shift  $\bar{v}_a$  of the attracted species relative to the hole, induces no hole asymmetry, but has two effects. One is a reduction in its flat-trapped density response to the hole potential  $\frac{dn_f}{d\varphi}$  and thus the magnitude of the contribution  $\tilde{f}_f$  to the required trapped depletion. In figure 3(a), this variation is plotted. The shift  $\bar{v}_a$  of the attracted species does not affect  $\tilde{f}_r$ , and since it acts in the same direction at low  $\bar{v}_a$  as  $\tilde{f}_f$ , the  $\tilde{f}_r$  comes to dominate the particle  $\tilde{f}$  contributions as  $\bar{v}_a$  increases toward unity. The other effect of increasing  $\bar{v}_a$  is to reduce the level of the flat trapped region to  $f(0) = \frac{1}{\sqrt{2\pi}} \exp(-\bar{v}_a^2/2)$ . As  $\bar{v}_a$  is increased, therefore, the hole amplitude must be reduced to avoid

the need for trapped deficit corresponding to an unphysical negative trapped distribution function. Fig. 3(b) shows the solutions of the equation  $\tilde{f}(\mathcal{E} = -\psi) + f(\mathcal{E} = 0) = 0$  (i.e. the total  $f_a(\mathcal{E} = -\psi) = 0$ ) using equations (10), and (12) together with the numerical evaluation of  $\tilde{f}$ . The result is  $\psi_{max}$ , the maximum value of  $\psi$  permitted by non-negativity of the (monotonic) total trapped distribution function. It shows that large  $\bar{v}_a$  permits only exponentially small potentials, because there is so small an attracted background  $f(0)$  in which to have a hole. Lower temperature ratio  $T_r/T_a$  gives a lower  $\psi_{max}$  because the repelled species response is stronger, requiring enhanced deficit  $|\tilde{f}|$  to overcome its influence.

#### IV. HOLE DYNAMICS AND STABILITY

In this section it is more convenient to speak in terms of velocity relative to some fixed frame, set by the particle velocity distributions, not the hole. In this frame the hole has a speed  $v_h$ . Electron hole speeds are often large compared with the thermal speed of the ions (the reflected species). In that case, repelled species response can be ignored.

When the repelled species response cannot be ignored however, because hole velocity is comparable to typical repelled velocity, repelled velocity distributions that are asymmetric (about the hole velocity) give rise to net reflection force on the hole, which causes the hole to accelerate. Such holes moving relative to a single shifted Maxwellian repelled species background distribution are thus not steady equilibria. Instead, the time dependence increases their effective velocity shift. Moreover holes with zero velocity relative to a Maxwellian repelled background, while they are (by symmetry) equilibria, are generally unstable to growing acceleration. This reflection mechanism was proposed as a possible cause of ion hole growth in early theory by Dupree<sup>4,33</sup> who analyzed the dynamics of holes treated as composite objects. There is good simulation evidence for the “self-acceleration” instability of electron holes<sup>34,35</sup>. Analytic theory of electron hole self-acceleration by interaction with ions agrees with simulations<sup>36</sup>.

Because velocity spread of ions is far smaller than electrons, ion holes essentially never move fast enough relative to the electron mean velocity to be able to ignore electron reflection. Therefore an important theoretical question arises as to whether and for how long ion holes, for which the repelled species is always significant, can exist. Acceleration of the hole velocity relative to attracted background (i.e.  $\dot{v}_h = -\dot{\bar{v}}_a$ ) causes evolution of the hole ampli-

tude  $\psi$ , both because the external distribution at  $f(v_h)$  changes, and because the amplitude must remain below the relevant  $\psi_{max}$  curve of Fig. 3(b). So once  $|\bar{v}_a|$ , the hole's speed relative to a Maxwellian attracted species' mean velocity, exceeds  $\sim 2(\times v_{ta})$  its amplitude becomes negligible. Unlike electron holes, this dissipation happens for ion holes long before their interaction with the repelled distribution ceases. The growth of the self-acceleration instability to speed  $\gtrsim 2$  is thus one important limit on the lifetime of an ion hole.

### A. Asymmetric Repelled Distributions

Asymmetric repelled species distribution (relative to the hole velocity  $v_h$ ) causes a difference in the distant repelled species density on either side of the hole. That requires a potential difference between the distant potentials on either side of the hole  $\Delta\varphi \neq 0$ , to satisfy distant neutrality<sup>18</sup>. The mechanism is illustrated in Fig. 4, which can be considered to show vertical slices through the contours of Fig. 1, except that a more complicated background repelled distribution  $f_{r\infty}(v_\infty)$  shown in the top panel Fig. 4(a) is considered. It represents the value of  $f(v)$  on incoming orbits ( $\text{sign}(v) = -\sigma_z$ ) at  $|z| = \infty$ . Fig. 4(b) shows local distributions  $f_r(z, v_r)$  at different potentials on either side of the hole potential peak ( $\text{sign}(z) = \sigma_z = \pm 1$ ). Reflected orbits for  $\sigma_z = -1$  (having negative velocity  $v - v_h$ ) are populated by incoming orbits at  $z = -\infty$  with positive velocity, while for  $\sigma_z = +1$  reflected orbits with positive velocity are populated by negative velocity orbits at  $z = \infty$ . Consequently there is a  $f_r(v_r)$  discontinuity at the energy equal to the potential peak  $\psi$ , which is at  $\frac{1}{2}(v_r - v_h)^2 = \psi - \varphi$ . As the position  $z$  moves inward from  $\pm\infty$  and the potential  $\varphi$  climbs, the discontinuity velocity moves toward  $v_h$  and exactly reaches it when  $\varphi = \psi$ . There are no  $z$  positions with  $\varphi > \psi$ .

The density is the integral  $\int f_r(v_r)dv_r$  which is evidently different for the two signs of  $\sigma_z$ , especially for small  $\varphi$ , as illustrated for a typical  $\varphi(z)$  shape in Fig. 5. Notice that the attracted species density remains a function purely of  $\varphi$ , and the deviation of the flat-trapped density  $n_f - 1$  (not including the trapped depletion  $\tilde{n}$ ) follows the shape of  $\varphi$ . The density difference results in an imbalanced net force  $F_r = \int n_r \frac{-d\varphi}{dz} dz = \sum_{\sigma_z=\pm 1} \int \sigma_z n_r d\varphi$  exerted on the repelled species, whose reaction on the potential itself must be balanced by momentum transfer to the attracted species.

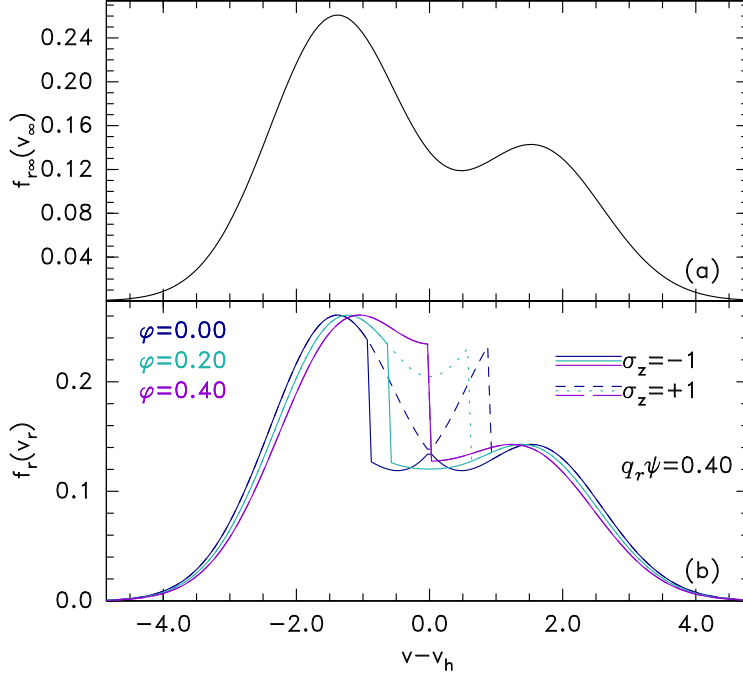


FIG. 4. (a) An example background repelled species distribution. (b) The corresponding local distribution functions at selected potentials  $\varphi$  on either side ( $\sigma_z = \pm 1$ ) of the potential peak (where  $\varphi = \psi$ ).

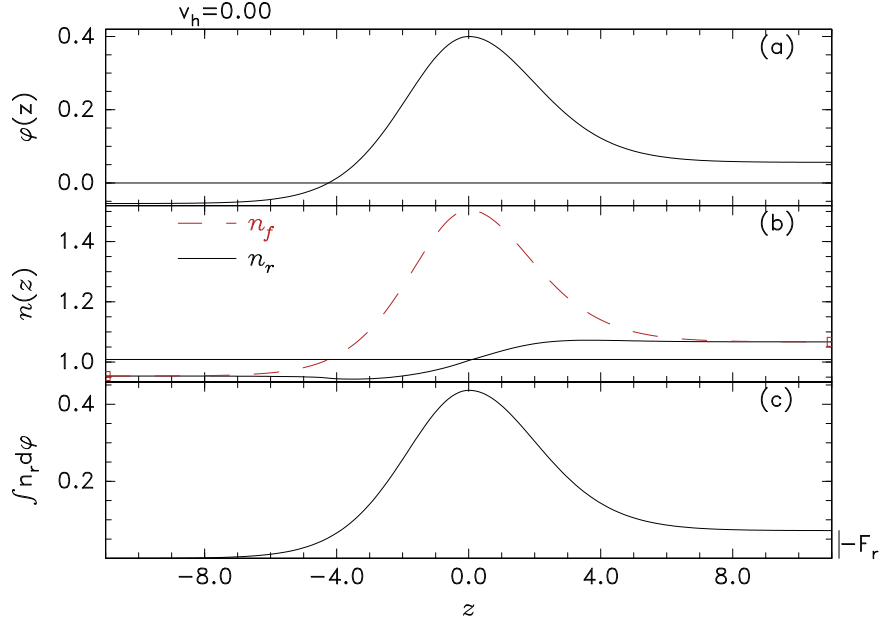


FIG. 5. Spatial dependence of (a) potential, (b) density, and (c) cumulative force  $\int_{-\infty}^z n_r d\varphi$  on the repelled species, for the repelled distribution of Fig. 4. .

## B. Reflection force balance

The dynamic behavior of a hole is determined by a balance of forces, which can be written as  $F_a + F_r = 0$ ; that is: the sum of the forces exerted by the hole on the attracted species plus the repelled species must be zero. In essence, the momentum of the electrostatic field is negligible; so it can support no reaction force. For electron holes of small potential amplitude ( $\psi \ll T$ ), these two forces have been calculated analytically in previous publications<sup>15,16</sup>. We here generalize to ion holes and to non-equilibrium situations, though the analysis is very similar. The mathematics is given only in outline, and relegated to Appendix B.

It is helpful to distinguish contributions to the density difference and force that arise from a possible potential difference  $\Delta\varphi = \varphi(+\infty) - \varphi(-\infty)$ , which are called extrinsic, from those, called intrinsic, which arise from asymmetries in the distributions even in the absence of potential asymmetry. The intrinsic force arises from the integral  $\int (n_r - n_a) \frac{d\varphi}{dz} dz$  over the  $z$ -range for which  $\varphi \geq |\Delta\varphi|/2$ . The extrinsic force comes from the  $z$ -range over which  $-|\Delta\varphi|/2 < \varphi < |\Delta\varphi|/2$ , which is only on the low potential side of the hole.

The attracted-species intrinsic force has been shown<sup>15</sup> to be proportional to the acceleration  $\dot{v}_h$  (in units of  $\sqrt{T_a/m_a}$ ) of the hole (in an inertial frame) giving an effective Newton's second law that attributes the momentum imparted to the trapped species to an effective mass:

$$\dot{P}_{aint} = M_a \dot{v}_h \quad \text{where} \quad M_a = \int \tilde{n} dz. \quad (14)$$

Here  $\dot{P}_{aint}$  is the intrinsic rate of attracted species momentum change, and  $M_a$  is the effective mass of the hole. The mass is negative, intuitively because the attracted species density deficit  $\tilde{n}$  is negative. The mass expression used here will be in a form which correctly accounts for any reflected species influence on the required density deficit ( $\tilde{n}$ ), eq. (41) of Hutchinson and Zhou<sup>15</sup>, not the alternative form eq. (33) for a fast electron hole in which ion perturbation can be ignored.

The repelled species intrinsic force arises to lowest order from reflection. It is independent of acceleration and its net depends on the antisymmetric part of the reflected velocity distribution function in the hole frame of reference. The resulting intrinsic momentum transfer rate to (i.e. reflection force on) the repelled species is

$$\dot{P}_{rint} = F_{rint} = \int_{\varphi \geq |\Delta\varphi|/2} -n_r \frac{d\varphi}{dz} dz, \quad (15)$$

where we recall that  $\varphi$  is normalized to  $T_a/|q|$ .

Approximating the distribution function,  $f_{r\infty}$  (in repelled species velocity units  $\sqrt{T_a/m_r}$ ) by a Taylor expansion, denoting differentiation with respect to velocity evaluated at the hole velocity (e.g.  $f'_r, f'''_r$ ), one can derive by integration explicit expressions for  $n_r$  and  $F_{rint}$ . See Appendix B. Although the force expressions to be cited are inexact for deep holes,  $\psi \sim 1$ , comparison with numerical calculation will show that the approximation is very good.

The combined (repelled plus attracted) extrinsic force can be obtained as the difference in the Maxwell stress across  $\Delta\varphi$ . The electric field is zero at  $\varphi = -|\Delta\varphi|$  (on the side with lower  $\varphi(\pm\infty)$ ), and, in view of the exponential potential decay in this region, at  $\varphi = +|\Delta\varphi|$  it is  $|E| = |\Delta\varphi|/\lambda$ , giving a force (stress difference)

$$\dot{P}_{ext} = F_{ext} = -\text{sign}(\Delta\varphi)|E|^2/2 = -\Delta\varphi|\Delta\varphi|/2\lambda^2. \quad (16)$$

It is shown in the Appendix that, to first order in  $\Delta\varphi$ ,  $F_{rint} + F_{ext} = [-4\psi^2 f'_r - \frac{8}{9}\psi^3 f'''_r]$ . So total momentum conservation is

$$0 = \dot{P}_{aint} + F_{rint} + F_{ext} = M_a \dot{v}_h + \left[ -4\psi^2 f'_r - \frac{8}{9}\psi^3 f'''_r \right]. \quad (17)$$

The potential difference across the hole  $\Delta\varphi$  is required to ensure distant neutrality,  $n_r - n_a = 0$  on both sides. Appendix B shows it is

$$\Delta\varphi = - \left( 4\psi f'_r + \frac{2}{3}\psi^2 f'''_r \right) / \left( \frac{1}{\lambda^2} - f'_r + \frac{1}{12}\psi f'''_r \right). \quad (18)$$

Equilibrium  $\dot{v}_h = 0$  requires  $f'_r$  to be first order small  $f'_r = -\frac{2}{9}f'''_r\psi$ , and that occurs only at specific discrete hole velocities  $v_{eq}$  close to extrema in the distribution shape. Here we concern ourselves in addition with non-equilibria in which  $\dot{v}_h \neq 0$ , and the acceleration will usually be well approximated by an expression linear in the difference  $v_h - v_{eq}$  between the hole velocity and a nearby equilibrium velocity.

### C. Numerical Calculation of Momentum Balance

The alternative to the small- $\psi$  analysis of the previous subsection is a full-scale numerical solution of the quasi-static forces and hole mass. The code previously used to find asymmetric electron hole equilibria and stability<sup>18</sup> accomplishes this task, but requires some modification to deal with non-equilibrium situations or shifted attracted species Maxwellians.

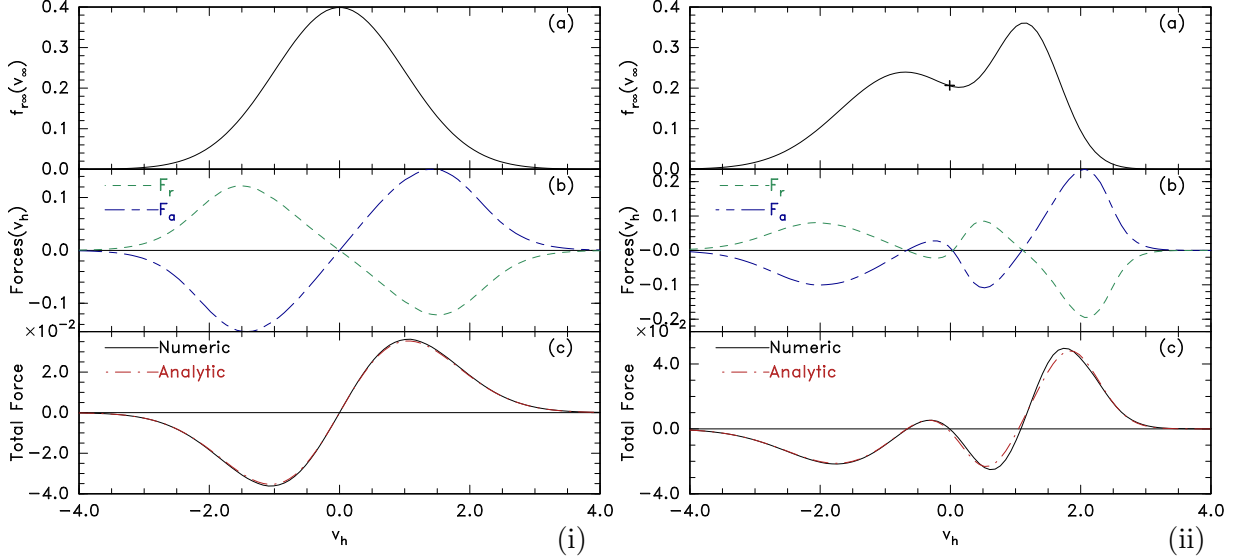


FIG. 6. Examples of force calculations showing: (a) the repelled distribution function vs. particle velocity, (b) vs. hole velocity the forces exerted on the repelled ( $F_r$ ) and attracted ( $F_a$ ) species, and (c) their sum, which is the total force, calculated numerically and compared with the analytic approximation  $[-4\psi^2 f_r' - \frac{8}{9}\psi^3 f_r''']$ . The attracted species has a Maxwellian distribution unshifted relative to the hole velocity  $v_h$ . The hole amplitude is  $\psi = 0.2$ .

In short, from a specified repelled distribution, in the hole frame, it calculates the repelled density everywhere. It then determines from the values  $n_r(\pm\infty)$  the required  $\Delta\phi$  for distant neutrality. The resulting forces on each species are  $-\int n q d\phi$ . The  $v_h$  can then be scanned, repeating this calculation, to find the equilibrium velocity  $v_{eq}$  at which the total force is zero.

Results are illustrated in Fig. 6. In it velocities are normalized to the repelled species, so for an ion hole the attracted species distribution is far narrower and would appear to be a delta function on the plot; in this calculation it is taken as a Maxwellian centered on the hole velocity. At left, Fig. 6(i), is shown the case for a simple Maxwellian repelled distribution. The total force is zero when  $v_h$  is at its centroid ( $v_{eq} = 0$ ), and rises initially linearly for non-zero  $v_h$  in a direction that would enhance  $|v_h|$  by acceleration. For large shifts the force returns to zero as the hole disengages from the repelled species and reflection ceases. At right, Fig. 6(ii), a double-humped repelled distribution is illustrated. There are then three zeroes of the total force that would correspond to equilibria. Those with positive force derivative are unstable (as in Fig. 6(i)), but the central zero with negative



derivative is stable. As for electron holes<sup>19,37</sup>, stability generally requires a local minimum in the repelled distribution and the hole velocity lying within it. The comparison between numerical and analytic results shows how good the analytic approximation is at  $\psi = 0.2$ . For higher potential amplitudes it deteriorates, and for lower amplitudes it becomes even better.

Nothing about the exact shape of the potential affects these forces. However, for non-equilibrium dynamics, the effective hole mass  $M_a = \int \tilde{n} dz$  depends upon the density spatial profile which depends on the potential profile. So to find it we need the total  $\varphi(z)$ . In the prior equilibrium publication the asymmetries were always small and it was sufficient to use an approximation to the  $\varphi(z)$  on the unspecified side. For strongly asymmetric holes this is not as well justified. So, instead, to obtain the dependence of  $M_a$  on  $v_h$ , the potential profile on the higher- $\varphi(\infty)$  side ( $\sigma_m$ ) is considered to be specified and hence  $\frac{d^2\varphi}{dz^2}$ . Thus  $\tilde{n} = n_r - n_f - \frac{d^2\varphi}{dz^2}$  is found and eq. (2) is evaluated to give  $\tilde{f}$  on this side. At the same  $\varphi$  on the other side  $\tilde{f}$  must be the same, because the trapped orbits are the same. Therefore on the  $-\sigma_m$  side Poisson's equation can be solved with specified densities  $n(\varphi)$ , to obtain  $z(\varphi)$ , complete the potential profile, and evaluate  $\int \tilde{n} dz$ .

A significant subtlety arises in the integral of eq. (2) when there is non-zero gradient  $\frac{dn_r}{dz}$  at the potential peak:  $z = 0$ ,  $\varphi = \psi$ . It is that since  $\frac{d\varphi}{dz}$  is zero there,  $\frac{dn_r}{d\varphi}$  is singular. Both  $n_r$  and  $n_f$  are bounded and have finite derivatives there; so if the potential shape is such that  $\frac{d^3\varphi}{dz^3} = \frac{dn_\varphi}{dz} = 0$ , then  $\frac{d\tilde{n}}{dz}$  is singular, and the integration to give  $\tilde{f}$  results in an unphysical cusp at  $z = 0$ ,  $v_a = 0$ . A simple potential specification such as  $\varphi = \psi \text{sech}^\ell(z/\ell\lambda)$ , for example, does give  $\frac{dn_\varphi}{dz} = 0$  because,  $\varphi$  being symmetric, has  $\frac{d^3\varphi}{dz^3}|_{z=0} = 0$ . It causes a cusp in  $f_{at}(v_a)$ , as illustrated by the dashed lines in Fig. 7. To avoid this unphysicality, a potential shape must be chosen that gives rise to a non-zero  $\frac{d^3\varphi}{dz^3}|_{z=0}$  value that exactly cancels the  $\frac{dn_r}{dz}$ . This requirement is, in effect, an additional constraint on  $\varphi$  profiles that are acceptable physically. It can be satisfied, for example, by adopting a potential form in which the  $z$ -variable is shifted by an increasing term:

$$\varphi(z) = \psi \text{sech}^4(h(z)) \quad \text{where} \quad h(z) = \frac{z}{4\lambda} + \frac{bz^2}{a^2 + z^2}, \quad (19)$$

which has  $\frac{d^3\varphi}{dz^3}|_{z=0} = -\frac{\psi 6b}{\lambda a^2}$ . We choose  $a = 1$  and set the  $b$  to cancel whatever  $\frac{dn_r}{dz}|_0$  is present. That gives the solid lines in Fig. 7.

Actually this correction has little influence on the force and hole mass calculation; and

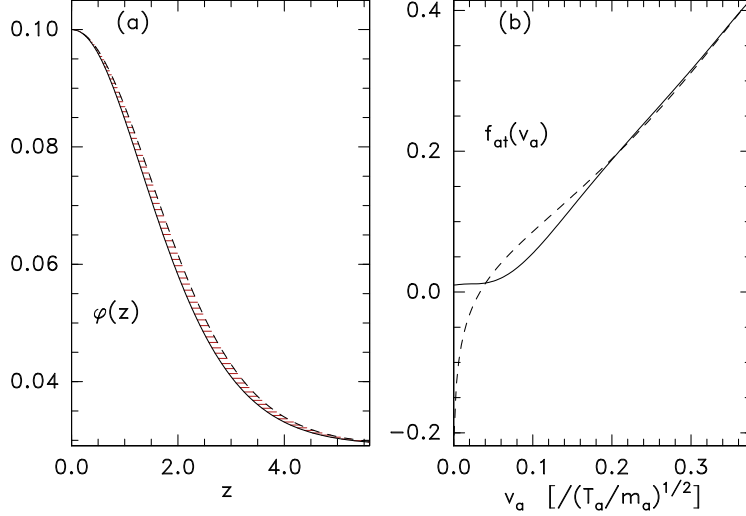


FIG. 7. Potential profile  $\varphi(z)$  and corresponding trapped distribution  $f_{at}(v_a)$  on the higher distant potential side of a hole with a single Maxwellian repelled species shifted by  $\bar{v}_r = -0.8$ , when the attracted species is unshifted Maxwellian and  $T_a/T_r = 1$ . Dashed lines are uncorrected and solid lines corrected by eq. (19).

omitting it would be a minor blemish on our main purpose. However, it appears to represent real physics, because it amounts to applying approximately a shift of the hole’s horizontal center  $\sum_{\sigma_z=\pm 1} z(\varphi)/2$  by an amount that depends on the height, being zero at the peak, but increasing to a constant at large  $|z|$ . That shape change could be described intuitively as the potential hill’s peak “leaning” toward the side with higher  $n(\infty)$ , but actually since the peak has been chosen to be at  $z = 0$  the base of the potential profile shifts in the opposite direction. These features are illustrated in Fig. 7. Even for this extremely asymmetric hole ( $v_h - \bar{v}_r = 0.8$ ) the shape distortion in  $\varphi$  is relatively modest. It is the way the hole “shares” its effective inertia across its entire extent, when it is being accelerated by asymmetric reflection of the repelled species. In the context of linearized stability analysis, this effect causes a distortion of the perturbation eigenstructure from the pure shiftmode. For the (two-dimensional) transverse instability, in which acceleration is caused by shear stress rather than repelled species reflection, this mode distortion has recently been treated via coupling of subsidiary eigenmodes<sup>38</sup>.

## D. Unstable acceleration

When the hole velocity lies a little above an equilibrium value  $v_{eq}$  that is near a local  $f_r$  maximum, the dominant term causing acceleration,  $-f_r'$ , gives a positive force on the particles and the reaction on the hole is negative. Then since  $M_a$  is also negative, the hole accelerates, moving its velocity away from the local  $f_r$  peak. Acceleration away from the peak also happens for a hole with velocity just below a local  $v_{eq}$ . Consequently although a hole with speed exactly at  $v_{eq}$  associated with a  $f_r$  maximum is in equilibrium, any velocity perturbation  $\Delta v_h = v_h - v_{eq}$  away from  $v_{eq}$  is unstable. On a single humped repelled velocity distribution, an unstable electron hole can accelerate till repelled species reflection ceases. But for an ion hole it disengages from the attracted distribution, and consequently collapses in amplitude, long before repelled species reflection ceases.

The growth rate of the instability near a local maximum at  $v_{eq}$  is determined to lowest order in  $\psi$  by the second derivative of the repelled distribution there  $f_r''$ , because  $f_r'(v_{eq} + \Delta v_h) \simeq f_r'(v_{eq}) + f_r''(v_{eq})\Delta v_h$ . Therefore to lowest order in  $\Delta v_h$

$$\dot{v}_h = \frac{d\Delta v_h}{dt} \simeq 4\psi^2 f_r''(v_{eq})\Delta v_h/M_a, \quad (20)$$

giving an exponential growth  $\Delta v_h \propto e^{\gamma t}$ , neglecting the dependence of  $M_a$  on  $v_h$ , with growth rate  $\gamma = 4\psi^2 f_r''(v_{eq})/M_a$ . Of course, near a local  $f_r$  minimum where  $f_r''$  is positive, by contrast,  $\gamma$  is negative, and in this approximation the hole velocity shift decays with time towards zero where  $v_h = v_{eq}$ .

Notice that this treatment regards the repelled distribution as exerting a force on an accelerating hole that is independent of the acceleration. That is hardly justifiable when the repelled species is ions because the timescale for repelled force ion equilibration is much longer than the typical  $1/\gamma$ . That is one reason why slow electron holes need a more elaborate treatment<sup>39</sup>. Ion holes, by contrast, accelerate far slower than electrons equilibrate; so the repelled species static approximation is very well justified.

In absolute units the  $f_r''$  being far smaller for ion holes than electron holes reduces the growth rate enough to justify the attracted species approximations as follows. In eq. (20) the time unit in  $d\Delta v_h/dt$  is  $\omega_{pa}^{-1}$ , but the velocity unit in  $f_r$  and its derivatives is  $\sqrt{T_a/m_r}$  which is large when the repelled species is electrons. Therefore a Maxwellian repelled distribution with temperature  $T_r$  has, at its peak,  $f_r'' = -(T_a/T_r)^{3/2}/\sqrt{2\pi} = -\theta^{-3/2}/\sqrt{2\pi}$ , and the

instability growth rate is  $\gamma = -(4/\sqrt{2\pi})\psi^2\theta^{-3/2}/M_a$  [ $\times\omega_{pa}$  in absolute units]. Since the hole mass ( $M_a$ ) units are the same for either species, the growth rate scaling like  $\psi^2\theta^{-3/2}/M_a$  attracted species time units gives growth rate slower in absolute time units for ion holes than electron holes by a factor  $\sim\sqrt{m_e/m_i}$ . Consequently the approximations for the attracted species are approximately as well justified for ion holes as they are for electron holes.

Quantitatively, taking  $\ell = 4$ , so  $\varphi = \psi \operatorname{sech}^4(z/4\lambda)$  which is a representative choice, and unshifted Maxwellians, a small- $\psi$  expansion gives

$$M_a = \int \tilde{n} dz = \left[ -\frac{16}{3}(1+1/\theta)\psi - \frac{512}{45\sqrt{\pi}}\psi^{3/2} + \frac{64}{35\theta^2}\psi^2 \right] (1+1/\theta)^{-1/2} + O(\psi^{5/2}), \quad (21)$$

which to leading order is  $M_a = -(16/3)\psi\sqrt{1+1/\theta}$ , giving

$$\gamma \simeq \frac{3}{4\sqrt{2\pi}} \frac{\psi}{\theta\sqrt{\theta+1}}. \quad (22)$$

For a small initial perturbation from equilibrium  $\Delta v_{h0}$  to grow to of order unity, taking the hole to the edge of the attracted velocity distribution, then requires a time  $t \simeq -\ln(\Delta v_{h0})/\gamma$  which for 10 e-foldings ( $\Delta v_{h0} \sim e^{-10}$ ) is  $t_{loss} \sim 10/\gamma \simeq 33\theta\sqrt{\theta+1}/\psi$  ( $\omega_{pa}^{-1}$ ).

Since the attracted deeply trapped particle bounce frequency is  $\omega_b \sim \sqrt{\psi}/2$  ( $\omega_{pa}$ ), there are many bounces in the time it takes for the hole to be accelerated to a velocity that causes it to dissipate:  $\omega_b t_{loss} \sim 33\theta\sqrt{\theta+1}/\sqrt{\psi} \gg 1$ . This inequality indicates that even though an ion hole is unstable in a Maxwellian background, it still retains its integrity long enough that the trapped dynamics is well represented by the equations we have been using. Its lifetime is also long enough to be observed as virtually steady (in its moving frame) by a satellite transiting at speeds at least comparable to the trapped particles.

Naturally if an ion hole lies in a locally flat  $f_r$  region or local minimum, its velocity is stable by the present analysis, and its lifetime could be much longer. We have not here addressed whether there are oscillating instabilities<sup>39</sup>, even when the hole lies in a minimum of  $f_r$ , arising from small phase-shifts in the attracted species response.

If an unstable ion hole is somehow born (created) at already substantial  $\Delta v_h \sim 1$  then only approximately one e-folding would be sufficient for it to dissipate by accelerating beyond the attracted distribution extent, in a time  $t_{loss} \sim 3\theta\sqrt{\theta+1}/\sqrt{\psi}$ . This might well be the relevant limit on hole life. However, provided the temperature ratio  $\theta = T_r/T_a$  is not too small, it would still be long enough for a typical satellite transit (at well above the ion thermal speed) to observe an approximately steady ion hole. Therefore the mere observation of an ion hole by a satellite does not rule out its accelerating at the rates calculated here.

Moreover, the growth rate being inversely proportional to  $\theta\sqrt{\theta+1}$  means it is reduced for an ion hole when the electron temperature is increased. Thus ion holes in higher  $T_e$  plasmas last longer before being collapsed by electron reflection acceleration. This effect is consistent with the tendency for ion holes to be more frequently observed in plasmas with higher  $T_i/T_e$ <sup>11</sup>, which is sometimes supposed to result from the erroneous  $\theta$  limit discussed in section III B.

## V. DISCUSSION

The phenomenon of transverse instability, which is known to be vital for electron holes, has not been addressed here for ion holes. There is every theoretical reason to suppose that ion holes are even more subject to it, because the effects of magnetization on the ion orbits are much reduced in the same plasma. That is because the ratio of ion plasma frequency to gyro frequency  $\omega_{pi}/\Omega_i$  is greater by the square root of the mass ratio than  $\omega_{pe}/\Omega_e$ . Thus in space plasmas ion holes hardly ever reside in a magnetic field strong enough that that  $\Omega_i$  exceeds approximately 1.5 times the ion bounce frequency  $\omega_b \sim \omega_{pi}\sqrt{\psi}/2$ . Instead the ions are effectively unmagnetized. The unmagnetized transverse instability fastest growth rate is<sup>40,41</sup> approximately  $\sqrt{\psi}/16$  ( $\omega_{pi}$  units for an ion hole). This exceeds the self-acceleration growth rate  $\gamma \simeq 0.3\psi/(\theta\sqrt{\theta+1})$  when  $\psi \lesssim 0.2\theta^2(\theta+1)$ . Thus small amplitude ion holes appear more likely to be limited by the transverse instability than self-acceleration, if they start from an equilibrium. An ion hole born already at a speed with substantial electron distribution gradient ( $f'$ ) would, however, accelerate promptly without having to wait for instability growth from noise, and if its amplitude is as great as  $\psi \sim 0.1$  might well collapse by acceleration before transverse instability breakup.

Although we have illustrated non-Maxwellian calculations, most of the explicit formulas here developed are given for Maxwellian distributions. That is not so great a weakness as might be supposed for space plasmas, even though they often have non-Maxwellian tails to their distributions, sometimes modelled by kappa functions (e.g.<sup>42</sup>). The reason is that electron influence on ion holes arises primarily from reflection, which occurs only for electron velocities close to the hole velocity, lying in the bulk of the electron distribution. Energetic tails on the wings of the electron distribution only marginally affect the hole equilibrium and give zero reflection force tending to accelerate it. Tails on the ion distribution might permit

ion holes to reach higher speed before dissipating because of the small background distribution in which they are holes, but they will still quite soon be limited by the mechanisms giving rise to Fig. 3(b), after some modest extension in  $v_a$ .

It should be emphasized that simulating ion holes by treating electrons via a fluid approximation, for example a Boltzmann density approximation, generally omits the asymmetric repelled species reflection effects that are the cause of ion hole acceleration discussed here. Thus, the electrons must include kinetic effects in their representation. The present analysis indicates that ion hole dynamics are affected only relatively little by the alternative simulation strategy of using a kinetic treatment of both species with unphysical increased electron mass to mitigate computational demands (e.g.<sup>9,43</sup>). For example, the unstable hole velocity growth rate (eq. 22) is unaffected, and ion holes rarely disengage with electrons. The same cannot be said about electron hole dynamics. They are greatly influenced by the mass ratio, since it dictates the velocity at which electron holes disengage from ions and cease to be accelerated.

The presumption made here that asymmetric background electron distribution functions are prescribed, becomes questionable for trains of ion holes, sometimes described as Cnoidal waves<sup>30</sup>. Electrons that reflect from one hole also reflect from an adjacent hole, and are therefore themselves trapped between two  $\varphi$  peaks. Their phase-space density is therefore not prescribed by some distant boundary condition. Trapping causes the reflecting electron orbits' distribution to be symmetrized in velocity. And (in contrast with electron holes) this repelled species symmetrization takes place on the electron transit timescale, which is much shorter than the ion timescale. In a train of similar holes making up a periodic wave, the result suppresses any reflection asymmetry force on an individual ion hole, and thus its tendency to accelerate. Addressing this situation is beyond the present scope.

**To summarize**, the equations governing equilibrium and dynamics of ion holes have been derived and solved analytically and numerically for representative potential shapes and distributions. Most of the mathematics is the same as for electron holes when expressed in appropriately normalized units. Ion holes can exist for a wide range of temperature ratios  $\theta = T_r/T_a$ , in contradiction of an erroneous but widely cited criterion. However, ion holes almost always give rise to electron reflection, in which case they are accelerated by asymmetry in the electron velocity distribution. Their lifetime is thereby limited to at most the time taken to accelerate out of the background ion velocity distribution, of order

$33\theta\sqrt{\theta+1}/\sqrt{\psi}$  ( $\omega_{pi}^{-1}$ ). This is nevertheless long enough for the quasi-static analysis presented to be reasonably appropriate, and for satellites to observe ion holes as approximately static in their rest frame.

## Appendix A: Waterbag Deficit Model

The ‘‘power deficit’’ model<sup>32</sup> consists of the assumption that the phase space density deficit is a specified function of energy

$$\tilde{f}(\mathcal{E}) \propto (\mathcal{E}_j - \mathcal{E})^\alpha \quad (\text{A1})$$

for  $\mathcal{E} < \mathcal{E}_j$  and zero for orbit energy  $\mathcal{E} \geq \mathcal{E}_j$ , where  $\mathcal{E}_j$  is a non-positive constant and  $\alpha \geq 0$  is the chosen power. This form allows for variable shape, but the enforced flat trapped  $f$  near the trapping boundary accounts for possible rapid energy diffusion there caused by stochasticity<sup>44</sup>. One can regard it as a generalization of the form used by Bohm and Gross<sup>45</sup>, which had  $\alpha = 1/2$ ,  $\mathcal{E}_j = 0$ . Notation is simplified by adopting the convention that any negative quantity to a real power (such as  $(\mathcal{E}_j - \mathcal{E})^\alpha$  when  $\mathcal{E} > \mathcal{E}_j$ ) is zero. The mathematical convenience of this power form is that it can be integrated to give

$$\tilde{n}(\varphi) = 2G \frac{\tilde{f}(-\psi)}{(\psi + \mathcal{E}_j)^\alpha} (\varphi + \mathcal{E}_j)^{\alpha+1/2}, \quad (\text{A2})$$

where  $G = \sqrt{\pi/2} \Gamma(\alpha + 1)/\Gamma(\alpha + 3/2)$ , and  $\Gamma$  is the standard Gamma function. This expression can further be integrated as

$$\int \tilde{n} d\varphi = 2G \frac{\tilde{f}(-\psi)}{(\psi + \mathcal{E}_j)^\alpha} \frac{(\varphi + \mathcal{E}_j)^{\alpha+3/2}}{\alpha + 3/2} \quad (\text{A3})$$

For small amplitude holes, we may approximate the rest of the density as  $n_f(\varphi) - n_r(\varphi) = K\varphi$ , where  $K$  is a positive constant. Then a closed form first integral of Poisson’s equation is

$$-\left(\frac{d\varphi}{dz}\right)^2 = 2 \int (n_r - n_f - \tilde{n}) d\varphi = -K\varphi^2 - 2G \frac{\tilde{f}(-\psi)}{(\psi + \mathcal{E}_j)^\alpha} \frac{(\varphi + \mathcal{E}_j)^{\alpha+3/2}}{\alpha + 3/2}. \quad (\text{A4})$$

The constant of integration is zero because  $\frac{d\varphi}{dz}|_{\varphi=0} = 0$ . At the potential peak ( $\varphi = \psi$ ),  $\frac{d\varphi}{dz}$  is again zero so

$$\tilde{f}(-\psi)/\psi^{1/2} = -K \frac{\alpha + 3/2}{4G} (1 + \mathcal{E}_j/\psi)^{-3/2}. \quad (\text{A5})$$

But the peak will be reached only if the derivative of the right hand side of eq. (A4) remains positive. Substituting from eq. (A5) into that derivative we obtain the condition  $K\psi(-2 + (\alpha + 3/2)(1 + \mathcal{E}_j/\psi) > 0$ , which is

$$\mathcal{E}_j/\psi < (\alpha - 1/2)/2. \quad (\text{A6})$$

This shows that for  $\alpha \rightarrow 0$ , which corresponds to a step function with transition at  $\mathcal{E}_j$ , i.e. a “waterbag” shape, the maximum permitted value of  $\mathcal{E}_j/\psi$  is  $-1/4$ . This case,  $\alpha = 0$ ,  $\mathcal{E}_j/\psi = -1/4$ , permits the highest value of  $\psi$  subject to the non-negativity constraint  $\tilde{f}(-\psi) \geq -f_a(0)$ . And the value is then

$$\psi_{max} = 3(Gf_a(0)/K)^2. \quad (\text{A7})$$

Substituting  $G = \sqrt{2}$  for  $\alpha = 0$ ,  $f_a(0) = 1/\sqrt{2\pi}$  for an unshifted Maxwellian, and  $K = 1 + T_a/T_r$  to account for the response of both species, we obtain

$$\psi_{max} = \frac{3}{\pi(1 + T_a/T_r)^2}. \quad (\text{A8})$$

## Appendix B: Analytic Density Difference and Force Expressions

Insofar as the antisymmetric part of the repelled species density can be represented through the first two nonzero terms in its distribution’s Taylor series in velocity:  $\Delta f_r = -(2f'v_{\mathcal{E}} + \frac{1}{3}f'''v_{\mathcal{E}}^3)$  — where for any potential or energy quantity (such as  $\mathcal{E}$ ) we use the notation  $v_{\mathcal{E}} \equiv \sqrt{2\mathcal{E}}$  — it is straightforward to show by integration [see Hutchinson<sup>18</sup> eq. 15] that the corresponding difference in repelled density between the two sides of the hole, at potential  $\varphi$  such that  $|\Delta\varphi|/2 \leq \varphi \leq \psi$ , is

$$\begin{aligned} \Delta n_{int}(\varphi) = & -2 \left[ v_{\psi-\varphi}v_{\psi} + v_{\varphi}^2 \ln\left(\frac{v_{\psi-\varphi} + v_{\psi}}{v_{\varphi}}\right) \right] f' \\ & - \frac{1}{12} \left[ v_{\psi-\varphi}v_{\psi}(2v_{\psi}^2 + 3v_{\varphi}^2) + 3v_{\varphi}^4 \ln\left(\frac{v_{\psi-\varphi} + v_{\psi}}{v_{\varphi}}\right) \right] f'''. \end{aligned} \quad (\text{B1})$$

The corresponding intrinsic force (difference) contributed from potentials above  $\varphi$  is  $F_{rint}(\varphi) = \int_{\varphi}^{\psi} \Delta n_{int}(\varphi)d\varphi = \frac{1}{2} \int_{v_{\varphi}^2}^{v_{\psi}^2} \Delta n_{int} dv_{\varphi}^2$  and the integrals can be evaluated to give

$$\begin{aligned} F_{rint}(\varphi) = & -\frac{1}{2} \left[ v_{\psi-\varphi}v_{\psi}(-2v_{\psi}^2 + v_{\varphi}^2) + v_{\varphi}^4 \ln\left(\frac{v_{\psi-\varphi} + v_{\psi}}{v_{\varphi}}\right) \right] f' \\ & - \frac{1}{24} \left[ \frac{1}{3}v_{\psi-\varphi}v_{\psi}(-8v_{\psi}^4 + 2v_{\psi}^2v_{\varphi}^2 + 3v_{\varphi}^4) + v_{\varphi}^6 \ln\left(\frac{v_{\psi-\varphi} + v_{\psi}}{v_{\varphi}}\right) \right] f'''. \end{aligned} \quad (\text{B2})$$



At  $\varphi = 0$  this expression gives  $F_{rint}(0) = -v_\psi^4 f' - \frac{1}{9} v_\psi^6 f'''$ ; and in equilibrium situations when  $\Delta\varphi$  is small, this is a sufficient approximation. However, since the higher potential side of the hill descends only to  $\varphi = \varphi_\Delta \equiv |\Delta\varphi|/2$ , the intrinsic force is actually  $F_{rint}(\varphi_\Delta)$  and far from equilibrium a more accurate expression is needed. The difference between the two expressions to first order in  $\Delta\varphi$  is

$$F_{rint}(0) - F_{rint}(\varphi_\Delta) = -2\psi|\Delta\varphi|f' - \frac{1}{3}\psi^2|\Delta\varphi|f'''. \quad (\text{B3})$$

And for non-equilibrium, accelerating, conditions this correction is required.

The total extrinsic force is  $F_{ext} = \int_{-\Delta\varphi/2}^{\Delta\varphi/2} (n_r - n_a) d\varphi$ , and if we approximate the densities as decaying with constant  $\varphi$ -derivative, giving  $n_r - n_a = 0$  at  $\varphi = -\varphi_\Delta$  then

$$n_r(\varphi) - n_a(\varphi) = \frac{n_r(\varphi_\Delta) - n_a(\varphi_\Delta)}{\Delta\varphi}(\varphi + \varphi_\Delta), \quad (\text{B4})$$

and the integral results in

$$F_{ext} = \Delta n(\varphi_\Delta)\varphi_\Delta = -2|\psi\Delta\varphi|f' - \frac{1}{3}|\psi^2\Delta\varphi|f'''. \quad (\text{B5})$$

This expression is precisely equal to the difference expression eq. (B3). Consequently, to first order in  $\Delta\varphi$ , the difference is cancelled and total force is

$$F_{rint}(|\Delta\varphi|/2) + F_{ext} = F_{rint}(0) = -4\psi^2 f' - \frac{1}{9}\psi^3 f''', \quad (\text{B6})$$

somewhat surprisingly independent of  $\Delta\varphi$ .

The intrinsic repelled density difference between the two sides of the hole at  $\varphi_\Delta$  where the sign of  $z$  is  $\sigma_z$  is obtained to first order in  $\Delta\varphi$  from eq. (B1) as

$$\sum_{\sigma_z=\pm 1} \sigma_z n_r(\varphi_\Delta) = \Delta n_{int}(\varphi_\Delta) = -(4\psi + |\Delta\varphi|)f' - \psi \left( \frac{2}{3}\psi + \frac{1}{12}|\Delta\varphi| \right) f'''. \quad (\text{B7})$$

Ignoring acceleration, there is no intrinsic difference in the attracted species density between the two sides of the hole at  $\varphi_\Delta$ . The ‘‘external’’ difference between repelled and attracted densities at this position can also be approximated to first order using eq. (9) and external neutrality at the lower side  $n_r(-\varphi_\Delta) - n_a(-\varphi_\Delta) = 0$  as

$$\Delta n_{ext}(\varphi_\Delta) = \text{sign}(\Delta\varphi)[n_r(\varphi_\Delta) - n_a(\varphi_\Delta)] \simeq \left( \frac{dn_r}{d\varphi} - \frac{dn_a}{d\varphi} \right) \Delta\varphi = -\frac{\Delta\varphi}{\lambda^2}. \quad (\text{B8})$$

Then neutrality at the higher  $\varphi(\infty)$  side requires  $\Delta n_{int} + \Delta n_{ext} = 0$ , which is

$$-(4\psi f' + \frac{2}{3}\psi^2 f''') + \Delta\varphi(f' - \frac{1}{12}\psi f''') - \frac{1}{\lambda^2} = 0, \quad (\text{B9})$$

giving eq. (18).

## ACKNOWLEDGMENTS

I am grateful to Ivan Vasko for helpful conversations. The code used to calculate and plot the figures is openly available at <https://github.com/ihutch/asymhill>.

## REFERENCES

- <sup>1</sup>I. B. Bernstein, J. M. Greene, and M. D. Kruskal, “Exact nonlinear plasma oscillations,” *Physical Review* **108**, 546–550 (1957).
- <sup>2</sup>S. Bujarbarua and H. Schamel, “Theory of finite-amplitude electron and ion holes,” *Journal of Plasma Physics* **25**, 515–529 (1981).
- <sup>3</sup>H. Schamel, “Stability of electron vortex structures in phase space,” *Physical Review Letters* **48**, 481–483 (1982).
- <sup>4</sup>T. H. Dupree, “Theory of phase-space density holes,” *Physics of Fluids* **25**, 277 (1982).
- <sup>5</sup>H. Pecseli, R. Armstrong, and J. Trulsen, “Experimental observations of ion phase-space vortices,” *Physics Letters A* **81**, 386–390 (1981).
- <sup>6</sup>H. Johnsen, H. L. Pécseli, and J. Trulsen, “Conditional eddies in plasma turbulence,” *Physics of Fluids* **30**, 2239–2254 (1987).
- <sup>7</sup>P. H. Sakanaka, “Beam-generated collisionless ion-acoustic shocks,” *Physics of Fluids* **15**, 1323–1327 (1972).
- <sup>8</sup>H. Pecseli, J. Trulsen, and R. Armstrong, “Formation of ion phase-space vortices,” *Physica Scripta* **29**, 241–253 (1984).
- <sup>9</sup>R. H. Berman, D. J. Tetreault, and T. H. Dupree, “Simulation of phase space hole growth and the development of intermittent plasma turbulence,” *Physics of Fluids* **28**, 155–176 (1985).
- <sup>10</sup>M. V. Goldman, D. L. Newman, and R. E. Ergun, “Phase-space holes due to electron and ion beams accelerated by a current-driven potential ramp,” *Nonlinear Processes in Geophysics* **10**, 37–44 (2003).
- <sup>11</sup>R. Wang, I. Y. Vasko, F. S. Mozer, S. D. Bale, I. V. Kuzichev, A. V. Artemyev, K. Steinvall, R. Ergun, B. Giles, Y. Khotyaintsev, P.-A. Lindqvist, C. T. Russell, and R. Strangeway, “Electrostatic solitary waves in the earth's bow shock: Nature, properties, lifetimes, and origin,” *Journal of Geophysical Research: Space Physics* **126**, e2021JA029357 (2021).

- <sup>12</sup>R. Wang, I. Y. Vasko, A. V. Artemyev, L. C. Holley, S. R. Kamaletdinov, A. Lotekar, and F. S. Mozer, “Multisatellite observations of ion holes in the earth's plasma sheet,” *Geophysical Research Letters* **49**, e2022GL097919 (2022).
- <sup>13</sup>F. S. Mozer, J. W. Bonnell, E. L. M. Hanson, L. C. Gasque, and I. Y. Vasko, “Nonlinear ion-acoustic waves, ion holes, and electron holes in the near-sun solar wind,” *The Astrophysical Journal* **911**, 89 (2021).
- <sup>14</sup>S. R. Bounds, R. F. Pfaff, S. F. Knowlton, F. S. Mozer, M. A. Temerin, and C. A. Kletzing, “Solitary potential structures associated with ion and electron beams near 1re altitude,” *Journal of Geophysical Research: Space Physics* **104**, 28709–28717 (1999).
- <sup>15</sup>I. H. Hutchinson and C. Zhou, “Plasma electron hole kinematics. I. Momentum conservation,” *Physics of Plasmas* **23**, 82101 (2016).
- <sup>16</sup>I. H. Hutchinson, “Electron holes in phase space: What they are and why they matter,” *Physics of Plasmas* **24**, 055601 (2017).
- <sup>17</sup>L. Muschietti and I. Roth, “Ion two-stream instabilities in the auroral acceleration zone,” *Journal of Geophysical Research: Space Physics* **113**, A08201 (2008).
- <sup>18</sup>I. H. Hutchinson, “Asymmetric one-dimensional slow electron holes,” *Phys. Rev. E* **104**, 055207 (2021).
- <sup>19</sup>I. H. Hutchinson, “How can slow plasma electron holes exist?” *Phys. Rev. E* **104**, 015208 (2021), <http://arxiv.org/abs/2104.13800>.
- <sup>20</sup>The Faddeeva function is related to the Plasma Dispersion function via  $Z(z) = i\sqrt{\pi}w(z)$  and to the Dawson integral function  $F(z)$  by  $w(iz) = 2F(z)$ . Its derivative is  $w'(z) = 2i/\sqrt{\pi} - 2zw(z)$ ; so  $-Z'(z)/2 = 1 + i\sqrt{\pi}zw(z)$ .
- <sup>21</sup>L.-J. Chen, D. Thouless, and J.-M. Tang, “Bernstein–Greene–Kruskal solitary waves in three-dimensional magnetized plasma,” *Physical Review E* **69**, 55401 (2004).
- <sup>22</sup>Those authors used a Gaussian potential shape so their  $\tilde{f}_\varphi$  is different and does not satisfy eq. (9).
- <sup>23</sup>Schamel et al proceed instead by the differential approach, specifying a negative temperature Maxwellian for trapped particles. They find by expansion at small  $\psi$  that  $\varphi = \psi \operatorname{sech}^4(z/4\lambda)$ , with  $\lambda^{-2} = 16b\sqrt{\psi}/15$  where  $b$  depends on the trapped temperature and  $\bar{v}_a$ , and that (13)  $1/\lambda^2 - 1/\theta + \frac{1}{2}Z'_r(\bar{v}_a/\sqrt{2}) = 0$ , which they call the nonlinear dispersion relation.
- <sup>24</sup>H. Schamel, “Theory of Electron Holes,” *Physica Scripta* **20**, 336–342 (1979).

- <sup>25</sup>H. Schamel and S. Bujarbarua, “Solitary plasma hole via ion-vortex distribution,” *Physics of Fluids* **23**, 2498–2499 (1980).
- <sup>26</sup>M. Hudson, W. Lotko, I. Roth, and E. Witt, “Solitary waves and double layers on auroral field lines,” *J Geophysical Research A* **88**, 916–926 (1983).
- <sup>27</sup>M. Buchanan and J. J. Doming, “Nonlinear waves in collisionless plasmas,” *Physics Letters A* **179**, 306–310 (1993).
- <sup>28</sup>J.-M. Grißmeier and H. Schamel, “Solitary holes of negative energy and their possible role in the nonlinear destabilization of plasmas,” *Physics of Plasmas* **9**, 2462–2465 (2002).
- <sup>29</sup>B. Eliasson, P. K. Shukla, and M. E. Dieckmann, “Theoretical and simulation studies of relativistic ion holes in astrophysical plasmas,” *New Journal of Physics* **8**, 55–55 (2006).
- <sup>30</sup>H. Schamel, N. Das, and P. Borah, “The privileged spectrum of cnoidal ion holes and its extension by imperfect ion trapping,” *Physics Letters A* **382**, 168–174 (2018).
- <sup>31</sup>A hole requires the inequality to be the opposite of the criterion for existence of what Stix<sup>46</sup> [section 9.14, equation 71] calls the “zero-damped ion acoustic wave”, because the sinusoidal shape of a wave makes  $\frac{1}{\lambda^2} \equiv \frac{1}{\phi} \frac{d^2\phi}{dz^2}$  negative, not positive.
- <sup>32</sup>I. H. Hutchinson, “Synthetic multidimensional plasma electron hole equilibria,” *Physics of Plasmas* **26**, 062036 (2021).
- <sup>33</sup>T. H. Dupree, “Growth of phase-space density holes,” *Physics of Fluids* **26**, 2460 (1983).
- <sup>34</sup>B. Eliasson and P. K. Shukla, “Dynamics of electron holes in an electron-oxygen-ion plasma.” *Physical Review Letters* **93**, 45001 (2004).
- <sup>35</sup>B. Eliasson and P. K. Shukla, “Formation and dynamics of coherent structures involving phase-space vortices in plasmas,” *Physics Reports* **422**, 225–290 (2006).
- <sup>36</sup>C. Zhou and I. H. Hutchinson, “Plasma electron hole kinematics. II. Hole tracking Particle-In-Cell simulation,” *Physics of Plasmas* **23**, 82102 (2016).
- <sup>37</sup>S. R. Kamaletdinov, I. H. Hutchinson, I. Y. Vasko, A. Artemyev, A. Lotekar, and F. Mozer, “Spacecraft observations and theoretical understanding of slow electron holes,” *Phys. Rev. Lett.* **127**, 165101 (2021).
- <sup>38</sup>X. Chen and I. H. Hutchinson, “Multimode theory of electron hole transverse instability,” *Journal of Plasma Physics* , to appear (2023).
- <sup>39</sup>I. Hutchinson, “Overstability of plasma slow electron holes,” *Journal of Plasma Physics* **88**, 555880101 (2022).

- <sup>40</sup>I. H. Hutchinson, “Kinematic Mechanism of Plasma Electron Hole Transverse Instability,” *Physical Review Letters* **120**, 205101 (2018).
- <sup>41</sup>I. H. Hutchinson, “Transverse instability of electron phase-space holes in multi-dimensional Maxwellian plasmas,” *Journal of Plasma Physics* **84**, 905840411 (2018), arXiv:1804.08594.
- <sup>42</sup>F. Haas, “Electron holes in a kappa distribution background with singularities,” *Physics of Plasma* **28**, 072110 (2021).
- <sup>43</sup>M. Lesur, P. H. Diamond, and Y. Kosuga, “Nonlinear current-driven ion-acoustic instability driven by phase-space structures,” *Plasma Physics and Controlled Fusion* **56**, 75005 (2014).
- <sup>44</sup>I. H. Hutchinson, “Particle trapping in axisymmetric electron holes,” *Journal of Geophysical Research: Space Physics* **125** (2020), 10.1029/2020JA028093, e2020JA028093 10.1029/2020JA028093, <https://agupubs.onlinelibrary.wiley.com/doi/pdf/10.1029/2020JA028093>.
- <sup>45</sup>D. Bohm and E. P. Gross, “Theory of plasma oscillations. a. origin of medium-like behavior,” *Physical Review* **75**, 1851–1864 (1949).
- <sup>46</sup>T. H. Stix, *The theory of plasma Waves* (McGraw-Hill, New York, 1962).